Levels of Structure Formation in Aqueous Solutions of Anisotropic Association Colloids Consisting of Rodlike Polyelectrolytes

M. Bockstaller,[†,‡] W. Köhler,[†] G. Wegner,[*,‡] D. Vlassopoulos,[§] and G. Fytas[§]

Physikalisches Institut, Universität Bayreuth, D-95440 Bayreuth, Germany; Max-Planck-Institut für Polymerforschung, Postfach 3148, D-55021 Mainz, Germany, and FORTH Institute for Electronic Structure and Laser, P.O. Box 1527, 71110 Heraklion, Crete, Greece

Received January 8, 2001; Revised Manuscript Received June 15, 2001

ABSTRACT: We report about structure formation in salt-free aqueous solutions of amphiphilic poly(*p*-phenylene)sulfonates (PPPs) that are models of rodlike polyelectrolytes. In water, PPPs form cylindrical micelles with constant diameter but variable length depending on the molar mass of PPPs. These micelles are the building blocks for the formation of higher ordered structures. The observed structures suggest attractive interactions between the cylindrical micelles in solution as predicted by counterion condensation theory for univalent counterions and for divalent counterions by computer simulations. By comparing the characteristics of structure formation for micelles of different length, the effect of the contour length of the cylindrical macroions on these attractive interactions might be revealed.

Introduction

Polyelectrolytes are of great importance in life sciences, and the ability of biogenic polymers to reproducibly form highly ordered structures by spontaneous self-assembly is fundamental to their biological function. Understanding and controlling the parameters that determine the structure formation process is of major interest. However, the process of structure formation of polyelectrolytes in solution depends on complicated coupling of short-range (excluded volume) and long-range (electrostatic) interactions, which restricts the theoretical treatment to plane, spherical, or cylindrical geometries. There is now considerable experimental and theoretical evidence from analytical theory[1,2] and numerical calculations[3,4] that attractive electrostatic interactions in systems of rodlike polyelectrolytes do exist and are of importance to structure formation.[5,6] These attractive interactions between rodlike polyelectrolytes are not captured by mean-field approaches like Debye−Hückel or Poisson−Boltzmann but can follow from correlated fluctuations in the distribution of the condensed counterions[1,3,4] and depend on the valency of the counterions as well as on the line charge density of the polyelectrolyte. For univalent counterions, the forces are exclusively repulsive. On the contrary, at intermediate distances identically charged rodlike polyions can experience attractive forces which are stronger for univalent counterions.[2] The restriction of the theoretical treatment to cylindrical geometry of the polyions, however, imposes serious constraints to real systems that might be used to compare theory and experiment. Because of their chemical simplicity and the possibility to selectively modify the chemical structure, synthetic stiff chain polymers are most promising systems to model the complex properties of biogenic polymers.

It was recently shown that dodecyl-substituted poly(*p*-phenylene)sulfonates (PPPs) spontaneously self-assemble into highly anisotropic cylindrical association colloids.[7] Within these aggregates the rigid PPPs align parallel to the axis of the cylinder with the ionic groups located at the outer surface. The hydrophobic aliphatic side chains fill the interior of the cylinder (Figure 1). Using static and dynamic light scattering, small-angle X-ray scattering, and electron microscopy, the association properties of two polymer samples differing in molar mass (12 and 27 kg/mol, abbreviated PPP12 and PPP27) have been characterized quantitatively. It has been found that these cylindrical aggregates are of remarkable stability over a broad concentration range with constant, molar mass independent, radial aggregation number. No individual chains could be observed at any concentration, meaning that the critical micelle concentration (cmc) is unobservably small.

With increasing concentration, these micelles undergo further association, and a concentration-dependent hierarchy of structures is observed as schematically shown in Figure 1 for the higher molar mass sample PPP27.

The single micelles found at very dilute solutions are the basic building blocks and exist in isotropic solution up to a concentration of $c = 0.02$ g/L.[7] At this concentration, the cylinders start to associate into clusters of ellipsoidal shape. Above $c = 1.1$ g/L, a nematic phase appears, which transforms into a hexagonal packing of the cylinders (i.e., a columnar phase) above $c = 8$ g/L. This hexagonal packing at high concentrations was already observed by Rulkens et al. up to concentrations as high as 270 g/L.[8] The shorter cylinders formed by the lower molar mass polymer PPP12 show significantly different structures when the concentration is increased. We will tentatively attribute this difference to a competition between repulsive electrostatic and attractive interactions mediated by the condensed counterions. The characterization of these consecutive levels of ordering, with the focus on PPP27, will be the subject of the present contribution.

Experimental Section

Materials. PPPs as shown in Figure 1 with molar mass $M = 27$ kg/mol (PPP27) have been studied. Details of the synthesis[9] and sample preparation[7,10] have been described elsewhere.

[†] Universität Bayreuth.
[‡] Max-Planck-Institut für Polymerforschung.
[§] FORTH Institute for Electronic Structure and Laser.
* Corresponding author.

10.1021/ma010027i CCC: $20.00
Published on Web 07/31/2001

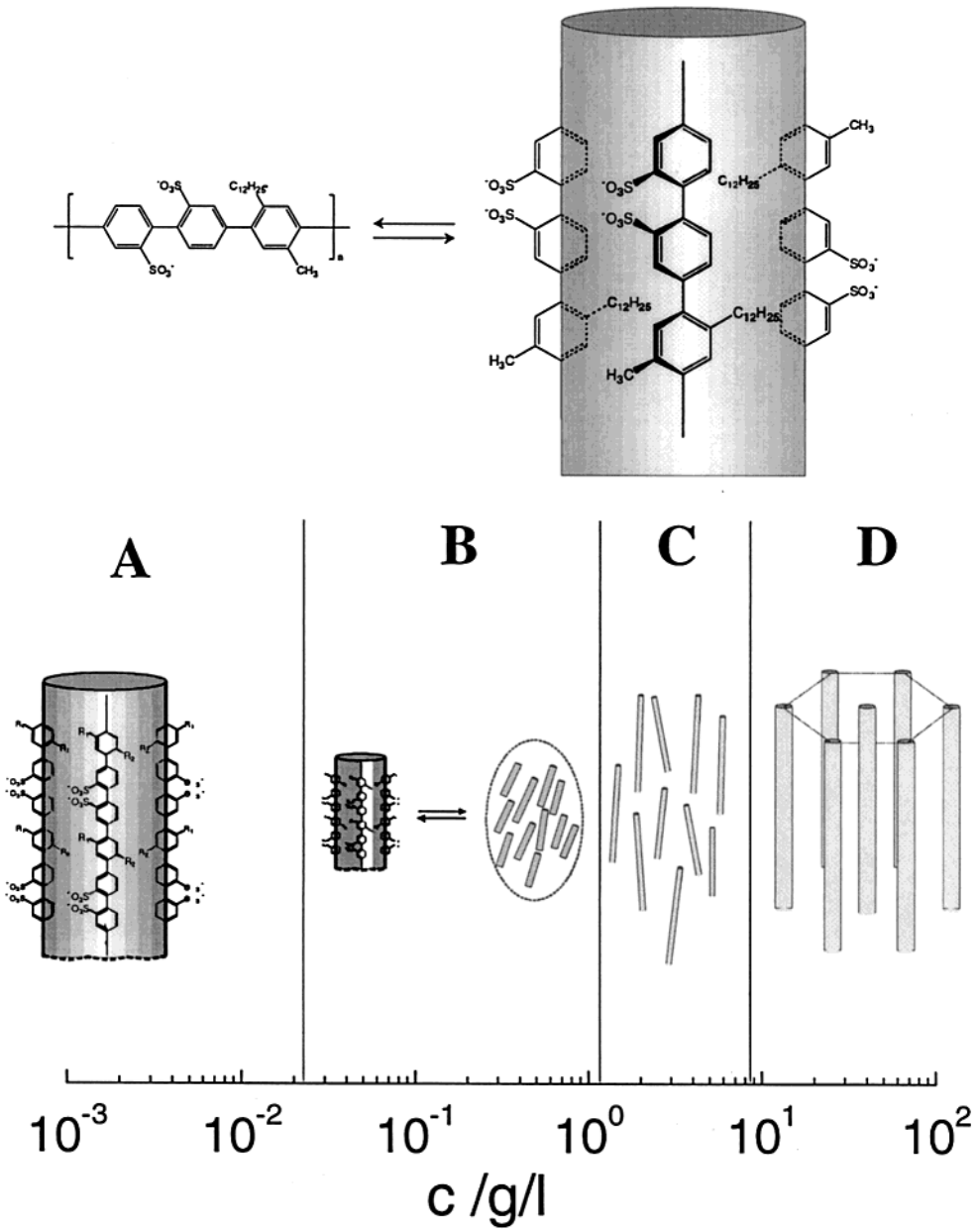

Figure 1. Chemical structure of the polyelectrolyte and schematic representation of the hierarchical structure formation of PPP27 in aqueous solution. PPP27 first forms cylindrical micelles (A) in which the hydrophobic side chains are oriented toward the interior. With increasing concentration, these micelles associate to form ellipsoidal clusters with internal lyotropic order (B), a nematic phase (C), and end up in a triangular lattice (D).

Viscometry. Viscosity measurements have been performed using an automatic Ubbelohde viscometer from SCHOTT-GERÄTE. The capillary diameter was chosen in order to avoid Hagenbach correction (diameter = 0.36 mm). All measurements have been carried out at $T = 20 \pm 0.01$ °C using a SCHOTT-GERÄTE thermostat (model 05392). The reduced viscosity was calculated by $\eta_{red} = t[c(t - t_0)]^{-1}$, where c is the polymer concentration and t and t_0 are the flow time of an equal volume solution and solvent through a capillary, respectively.[11]

Shear Rheology. The shear rate dependence of the solution viscosity was determined using a Rheometric Scientific constant strain rheometer (model ARES-HR) with a very sensitive dual range force rebalance transducer 100FRNT$_1$ in the Couette geometry. All measurements were carried out at $T = 20 \pm 0.01$ °C in a water-saturated atmosphere.

Photon Correlation Spectroscopy. Details of the photon correlation spectroscopy measurements can be found in ref 7. For analysis of the experimental correlation function $C(q,t) = \alpha g_1(q,t)$, where $g_1(q,t)$ is the electric field autocorrelation function and α is the fraction of the total scattered intensity arising from fluctuations with correlation times longer than 10^{-7} s, we have employed inverse Laplace transformation using the constraint regularized CONTIN method.[12] This method assumes that $C(q,t)$ can be represented by a superposition of exponentials

$$C(q,t) = \int_{-\infty}^{\infty} H_\tau(\ln \tau) \exp[-t/\tau] \, d(\ln \tau) \qquad (1)$$

which determines a continuous spectrum of relaxation times $H_\tau(\ln \tau)$. The characteristic relaxation times correspond to the maxima of $H_\tau(\ln \tau)$.

Small-Angle X-ray Scattering. The SAXS measurements were performed using a Cu−Kα X-ray source with $\lambda = 0.154$ nm and a Kratky compact camera. For photon counting, an array detector OED50M (Braun) was employed. For enhanced accuracy, a flow capillary has been designed to avoid setup changes during the measurement.

Polarization Microscopy. Microscopic experiments were carried out using a ZEISS Axiophot photomicroscope with a

LINKAM THM 600 heating table. For measurements of the polarized light, a UD 40 objective (ZEISS) combined with slide polarizers was used.

Results and Discussion

Viscometry. The reduced viscosity of polymer solutions yields information about the dissipative characteristics of a solute related to hydrodynamic shape and interaction potentials of the particles in solution.[13] The reduced viscosity is expected to be proportional to the polymer concentration for neutral polymers. For electrostatically interacting particles, η_r decreases with c, and it has been shown[14] that the reduced viscosity follows the empirical Fuoss−Strauss law

$$\eta_{red} = \frac{A}{1 + B\sqrt{c}} \tag{2}$$

where A and B are size-dependent constants.[15] Cohen et al. suggested that this behavior could be explained on the basis of liquid-state "mode-coupling" theories developed for the study of spherical charged colloids.[14,16] In the weak coupling regime, it was shown that the viscosity of a suspension of spherical charged particles is given by

$$\eta = \eta_s R c^2 Z^4 l_B \kappa^{-3} \tag{3}$$

where Z is the charge and R the hydrodynamic radius of the polyion. η and η_s are the viscosity of the solution and solvent, respectively. The Bjerrum length $l_B = e^2/(4\pi\epsilon_0\epsilon k_B T)$, with e the elementary charge, $k_B T$ the thermal energy, ϵ_0 the permittivity of vacuum, and ϵ the dielectric constant of the solvent, characterizes the strength of the electrostatic interactions in the solvent. The inverse Debye screening length is given as $\kappa = 4\pi l_B I$ with $I = 0.5\sum_i Z_I^2 c_i$ being the ionic strength (Z_i is the valence and c_i the concentration of species i). Cohen et al. pointed out that eq 3 is similar to the experimentally observed eq 2, if the polymer chain is assumed to bear the effective charge $Z^* = \sqrt{fN}$, where f is the degree of ionization and N is the degree of polymerization.

Figure 2 shows the reduced viscosity of PPP27 in water and methanol as a function of concentration. As shown by the solid lines, the reduced viscosity of the polymer samples in methanol can be described by the Fuoss−Strauss relation (eq 2), indicating domination of the repulsive interactions as expected for like charged polyions.[17] This result can be related to light scattering studies of Liu et al.,[18] who investigated the structure formation properties of PPPs like polymers in methanol and who concluded that in methanol PPPs exist essentially as single macromolecules.

In aqueous solution, however, the concentration dependence of η_{red} of sample PPP27 strongly deviates from the one expected for dominating repulsive interactions. The reduced viscosity monotonically increases with concentration, showing a smeared out step at $c \approx 0.02$ g/L, and it diverges for $c > 0.8$ g/L. It is noted that the deviation from the expected polyelectrolyte behavior at dilute solutions is also revealed by the light scattering from dilute PPPs solutions, displaying a positive second virial coefficient A_2 for PPP12[7] and a negative one for PPP27.

Figure 3 shows the absolute viscosity for aqueous solutions of PPP27 with different concentrations as a function of shear rate. Non-Newtonian behavior is

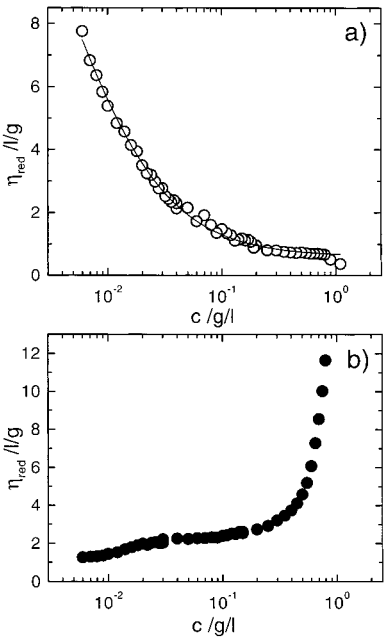

Figure 2. (a) Reduced viscosity of PPP27 in methanol (○). The solid line in (a) represents a least-squares fit according to eq 2 with fit parameters $A = 100$ g/L and $B = 150$ (g/L)$^{-1/2}$. (b) Reduced viscosity of PPP27 (●) in water. η_{red} exhibits an "anti-polyelectrolyte" effect.

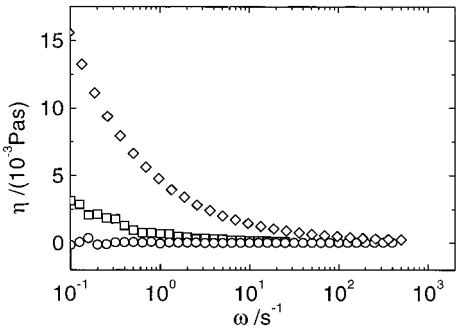

Figure 3. Shear rate dependence of aqueous solutions of PPP27 at $c = 0.86$ (○), 1.17 (□), and 2.81 g/L (◇). The onset of nonlinear viscoelasticity ($\eta(0) \neq \eta(\omega)$) at $c \approx 1.17$ g/L marks the isotropic → nematic phase transition.

observed for sample PPP27 for $c \geq 0.87$ g/L. As will be shown below, this corresponds to the formation of a nematic phase that can be observed in the optical microscope with crossed polarizers. The smeared out step at $c = 0.02$ g/L in Figure 2a indicates the formation of lyotropic clusters of cylindrical micelles which are precursors to the nematic phase. Since it has been shown that PPP27 in aqueous solution forms micelles of diameter $d = 3.4$ nm and length $L_N = 280$ nm,[7] whereas no such micelle formation could be observed in methanol,[18] we assume the formation of micelles to be responsible for the different rheological properties.

Static Light Scattering. Figure 4 shows a plot of the reduced total scattered intensity $R(0)/Kc$ for PPP27 in the range $0.001 \leq c \leq 0.5$ g/L, where $R(0)$ is the Rayleigh ratio in the limit $q \rightarrow 0$. In agreement with the smeared out step of the reduced viscosity (Figure 2), there is a characteristic bend in the concentration dependence of $R(q)/Kc$ at $c \approx 0.02$ g/L. Within concentration regime A, the intensity increases with concentration, and from the slope of $Kc/R(0)$ vs c the second viral coefficient $A_2 = -1.84 \times 10^5$ L mol g^{-2} is obtained, indicating attractive interactions between the solute

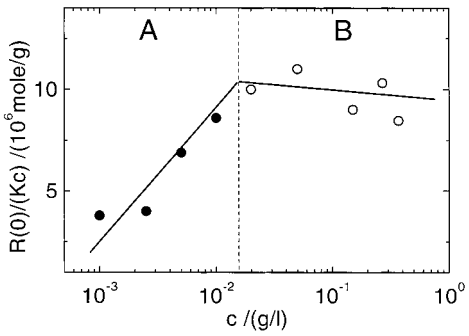

Figure 4. $R(0)/(Kc)$ as a function of concentration of aqueous solutions of PPP27. The bend in scattering intensity at c = 0.02 g/L indicates the crossover from regime A to regime B.

particles. In regime A, the structure formation properties of PPP27 have been studied extensively. By combining scattering and electron microscopy techniques, it was shown that an isotropic solution of cylindrical micelles of PPPs with diameter $d = 3.4$ nm, length $L_N \approx 280$ nm, and molar mass $M_W = 3.6 \times 10^6$ g/mol does exist.[7]

For rodlike polyelectrolytes, A_2 is positive. Neglecting any end effects, Odjik derives

$$A_2 = \frac{\pi}{4} L^2 d_{\text{eff}} \tag{4}$$

where L is the length and $d_{\text{eff}} \approx \kappa^{-1}(0.7704 + \log(2\pi\xi^2 l_B \kappa^{-1}))$ (with ξ being the effective charge density) is the effective diameter of the charged rod.[19] Therefore, the results indicate that mean-field approaches may not always be sufficient to describe the interactions between polyelectrolytes in solution.

The sudden change of the rate of increase of the scattered intensity with c characterizes the transition from regime A to regime B. After reaching a maximum at $c = 0.02$ g/L, the scattering intensity slowly decreases with c. The concentration dependence as shown in Figure 4 resembles the one expected for surfactants, which spontaneously form micellar aggregates once the cmc is reached.[20,21] To emphasize this analogy, $c_{\text{crit}} = 0.02$ g/L will be called the critical concentration in the following. As will be shown by dynamic experiments, this concentration marks the onset of the formation of ellipsoidal clusters consisting of cylindrical micelles (see Figure 1). Above $c = 0.5$ g/L, a quantitative analysis of the scattering experiments was not possible due to multiple scattering. Information about the structure formation for $c > 0.5$ g/L has been obtained by microscopy, X-ray scattering, and rheological experiments (see below).

Photon Correlation Spectroscopy. Structure analysis of different aggregates coexisting in solution—corresponding to different levels of association—can be performed by photon correlation spectroscopy, since the contribution of the different particles to the scattering can be separated in the time domain.[7,10,22] Size and shape determination is possible by fitting the angular dependence of the scattering contribution of a dynamic mode to different theoretical models (form factors). The comparison between calculated D^{th} and experimentally measured translational diffusion coefficients D yields independent information about the hydrodynamic size and shape of the solute. Information about the internal structure of the aggregates can be obtained by depolarized light scattering, since it reflects the optical anisotropy which can be compared to the form anisotropy. To simplify the analysis, we will treat D at $q = 0$ as self-diffusion coefficient of the corresponding particles. This will lead to results that correspond well with the ones obtained from electron microscopy.[7] Corrections due to finite concentration will be neglected.

Parts a and b of Figure 5 show the relaxation function $C_{VV}(q,t)$ along with the corresponding distribution of relaxation times $H(\ln \tau)$ at $q = 8.31 \times 10^6$ m^{-1} for the isotropic (VV) scattering component of a salt-free aqueous solution of PPP27 at $c = 0.008$ g/L and $c = 0.47$ g/L. Characteristic for concentration regime B (Figure 4) is the appearance of an additional slow mode above $c_{\text{crit}} = 0.02$ g/L, which accounts for the main fraction to the total scattering intensity (cf. the areas of the $H(\ln \tau)$ peaks).

As can be seen by comparison of parts b and c of Figure 5, this slow mode is also active in the depolarized scattering, implying that these moieties have to be anisotropic. The single diffusive relaxation process at $c = 0.008$ g/L corresponds to freely diffusing micellar aggregates of cylindrical shape consisting of about 80 polymer chains.[7] The presence of two distinct self-assembled aggregates at $c > c_{\text{crit}}$ that contribute to $R(q)$ is demonstrated in the bimodal relaxation function in Figure 5b. From the relaxation time distribution $H(\ln \tau)$, the contribution of a dynamic mode i to the total $R(q)$ can by calculated by

$$R_i(q) = R(q) \int_{\ln \tau_{\min}}^{\ln \tau_{\max}} H(\ln \tau)\, \mathrm{d}(\ln \tau) \tag{5}$$

$\tau_{\min}$ and $\tau_{\max}$ correspond to the minimum and maximum relaxation time of mode i in the relaxation time spectrum. Figure 6 shows the q dependence of the fraction of $R(q)$ due to the fast and slow diffusing species as calculated by eq 5. As confirmed by the q^2 dependence of the relaxation rates (inset of Figure 6), both modes correspond to distinct diffusing entities. The angular dependence of the intensity of the fast mode can be represented by the thin-rigid-rod scattering function[23]

$$P_r(qL) = \frac{2}{qL} \int_0^{qL} \frac{\sin z}{z}\, \mathrm{d}z - \left(\frac{\sin qL/2}{qL/2}\right)^2 \tag{6}$$

An analysis according to eq 6 yields a length of $L = 500$ nm for the fast diffusing species, which corresponds to the first level of association, the cylindrical micelles. They are also present at concentrations below c_{crit} and were characterized rigorously in a previous publication.[7] There, the existence of cylindrical micelles with constant strand aggregation number below and above c_{crit} was also confirmed by electron microscopy after cryofixation.

The larger fraction of $R(q)$ above c_{crit} is due to the slow diffusing species and exhibits a strong q dependence. The angular dependence of this $R_{\text{slow}}(q)$ can be represented assuming a prolate ellipsoidal geometry, for which the form factor is written as

$$P_{\text{ell}}(u) = \frac{9\pi}{2} \int_0^{\pi/2} \left(\frac{J_{3/2}[u]}{u^3}\right) \cos\beta\, \mathrm{d}\beta$$

$$u = qa\sqrt{\cos^2\beta + \left(\frac{b}{a}\right)^2 \sin^2\beta} \tag{7}$$

a and b refer to the long and the short axis, respectively.[24] Analyzing the data displayed in Figure 6 with eq 7 yields $a = 600$ nm and $b = 400$ nm. For scatterers

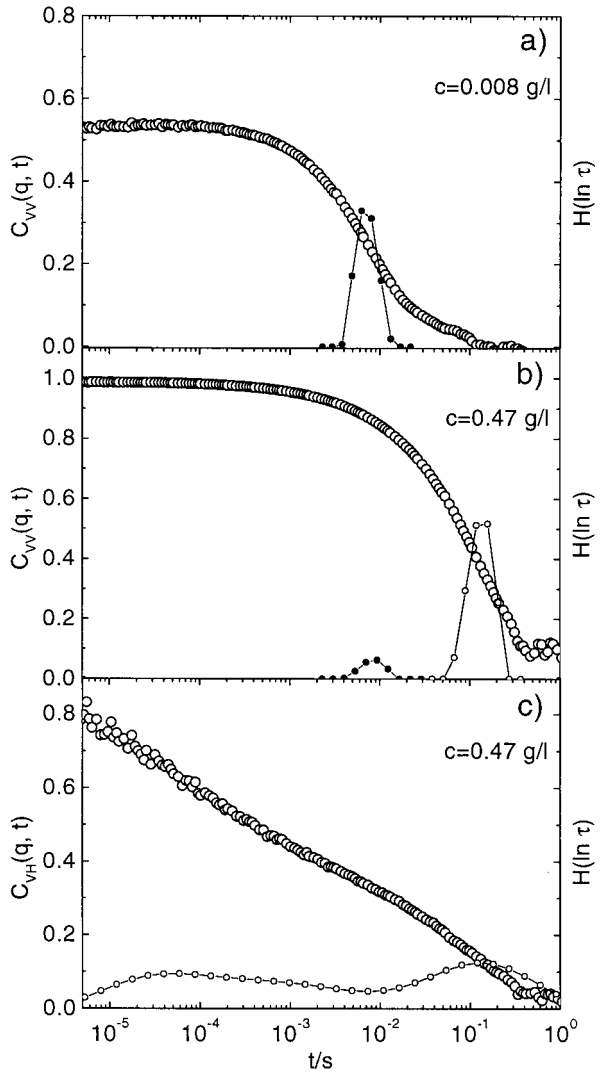

Figure 5. Relaxation function $C(q,t)$ for concentration (a, b) and orientation (c) fluctuations at $q = 8.15 \times 10^6$ m^{-1} in salt-free aqueous solutions of PPP27 at different concentrations. The filled and the open symbols of $H(\ln \tau)$ in (a, b) correspond to the cylindrical micelles A and the lyotropic clusters B, respectively.

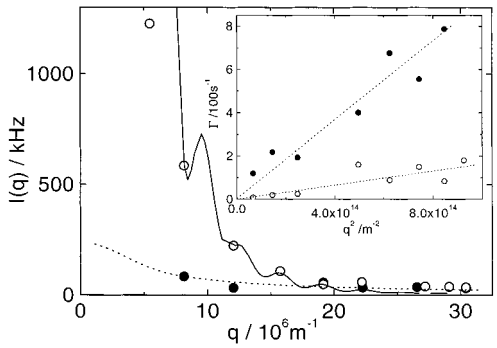

Figure 6. Scattering contribution (eq 5) of the fast (●) and slow (○) mode shown in Figure 5b along with calculated scattering functions for a rod (dashed line) of length $L = 500$ nm (eq 6) and ellipsoid (solid line) with $a = 600$, $b = 400$ nm (eq 7). The diffusive nature of the fast and slow processes is shown in the inset as Γ vs q^2.

of this size ($qR > 4$), the field in the interior of the particle may be effected by internal reflections. To justify the ellipsoidal geometry of the slowly diffusing species, a comparison of the expected and experimentally measured dynamics is necessary. The translational

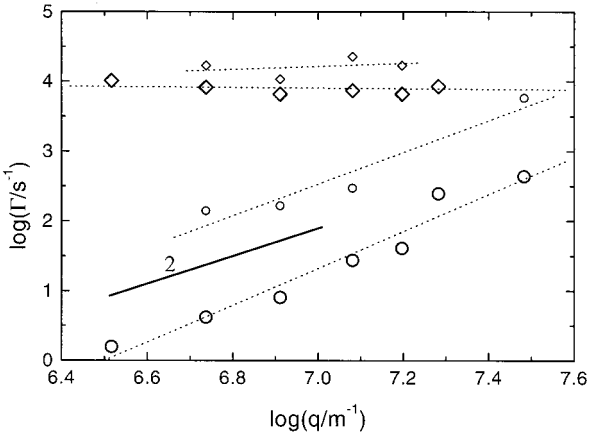

Figure 7. q dependence of relaxation rate of fast (small ◇, large ◇) and slow (small ○, large ○) mode in the orientation relaxation function of aqueous solutions of PPP27 at $c = 0.09$ g/L (small symbols) and $c = 0.47$ g/L (large symbols). The dynamics of the fast process is q-independent.

Table 1. Size of the Self-Assembled Structures in PPP27

	static		dynamic	
c, g/L	a, nm	b, nm	D^{exp}, m^2/s	D^{th}, m^2/s
0.09	300	120	9.4×10^{-13}	1.2×10^{-12}
0.21	450	350	3.5×10^{-13}	2.3×10^{-13}
0.31	350	250	3.2×10^{-13}	5.9×10^{-13}
0.47	600	400	1.4×10^{-13}	2.6×10^{-13}

diffusion coefficient of prolate ellipsoids can be calculated from the Einstein relation[25]

$$D = \frac{k_B T}{f} \tag{8}$$

The friction coefficient f of hydrodynamically interacting prolate ellipsoids has been derived by Perrin:[26]

$$f = \frac{6\pi\eta_S a}{\sqrt{1 - b^2/a^2}\,\ln\dfrac{1 + \sqrt{1 - b^2/a^2}}{b/a}} \tag{9}$$

For $c = 0.47$ g/L, the diffusion coefficient of the slowly diffusing species is obtained to be $D = 1.4 \times 10^{-13}$ m^2/s, which is close to the expected value $D^{th} = 2.6 \times 10^{-13}$ m^2/s for prolate ellipsoids with $a = 600$ nm and $b = 400$ nm, which also describe the intensity of the slow process (Figure 6). Table 1 summarizes the geometrical dimensions of the slowly diffusing species as determined by fitting the angular dependence of $R_{slow}(q)$ with the form factor of ellipsoidal scatterers (eq 7), as well as the expected (eq 9) and experimentally measured translational diffusion coefficients.

For aqueous solutions of PPP27, dynamic (in the PCS time window) depolarized scattering was observed already at low concentrations ($c \geq 0.05$ g/L). The sensitivity of depolarized scattering to nonspherical shapes is advantageous in the study of association processes. It is, however, not often employed. $C_{VH}(q,t)$ as shown in Figure 5c exhibits two processes with distinctly different q dependence. Whereas the slow process has a diffusive rate $\Gamma \propto q^2$, the relaxation rate of the fast process is q-independent (see also Figure 7).

Slow Dynamics. By comparison of Figure 5c with the isotropic relaxation function in Figure 5b, it can be seen that Γ_{VH} and Γ_{VV} are almost identical for the slow process. This finding implies that the scatterers are

large enough, so that the slow rotational diffusion D_r in $\Gamma_{VH} = 6D_r + Dq^2$ can be neglected. Information about the internal structure of the slowly diffusing species can be obtained by comparing the expected with the experimentally measured depolarized scattering intensity. The contribution of the slow diffusing scatterers to the total depolarized scattering intensity is calculated according to eq 5, revealing that 90% of the depolarized scattered intensity is due to the slowly diffusing entities. The strong VH scattering can hardly be rationalized by the almost spherical geometry of the slowly diffusing species as obtained by the analysis of the VV scattering. Since the depolarized scattering is sensitive to the optical anisotropy of the scatterers, rather than to their form anisotropy, we conclude that the slowly diffusing species correspond to ellipsoidal clusters of almost spherical shape but with preferential ordering of the cylindrical micelles constituting the interior. This interpretation is confirmed by electron micrographs after cryofixation which have already been published.[7] The picture of these lyotropic clusters is schematically shown in Figure 1 (regime B). It is probably worth mentioning that in the present case dynamic anisotropic (VH) light scattering arises from the diffusion of these lyotropic objects seen via the anisotropy of the constituent cylindrical micelles. The much faster collective orientation dynamics of the latter is responsible for the fast process of Figure 5c.

Fast Dynamics. The fast relaxation dynamics in VH scattering geometry is characterized by a q-independent rate, as well as a rather broad shape as reflected in the position and width of the $H(\ln \tau)$ peak in Figure 5c. It is not active in the isotropic scattering. Moreover, the relaxation rate is insensitive to concentration variation in contrast to the slowing down of the slow process as shown in Figure 7. The broad spectrum of relaxation times of the fast process can hardly be rationalized without involving extensive cooperativity of orientational fluctuations. Assuming ellipsoidal clusters with a lyotropic ordering of the cylindrical micelles which fill the interior, it is conceivable that the constituent cylinders can undergo collective orientational motions similar to the dynamics of a nematic phase.[27] Following this picture, the results indicate an almost unchanged internal structure of the lyotropic clusters over a broad concentration range. It should be mentioned that similar broad orientation relaxation functions were observed for the neutral precursors of PPPs in nondilute solutions.[28]

Polarization Microscopy. The alignment of optically anisotropic molecules can be detected by polarization microscopy. A preferential orientation of the mesogens along a director results in birefringence due to a directional dependence of the refractive index, which results in characteristic textures to be observed in an optical microscope using crossed polarizers.[29] Figure 8 shows a micrograph of an aqueous solution of PPP27 at $c = 4.3$ g/L when observed through an optical microscope using crossed polarizers. The observed Schlieren textures indicate the formation of a nematic phase. No birefringence could be observed below $c = 1.1$ g/L. It is noted that the appearance of Schlieren textures ($c \approx 1.1$ g/L) coincides with the onset of a shear rate dependence of the viscosity as shown in Figure 3. The divergence of viscosity at shear rate $\dot{\gamma} = 0$ originates in the collective motions of the orientationally correlated mesogens in solution and is expected for a nematic structure of the solute.[27]

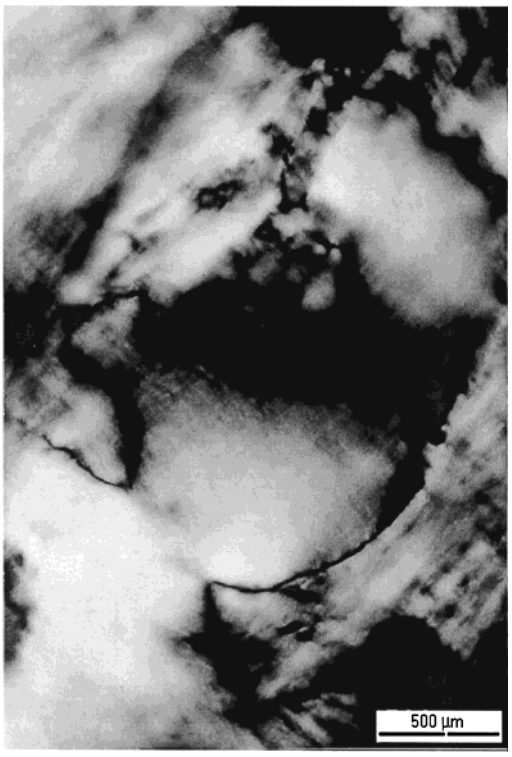

Figure 8. Micrograph of an aqueous solution of PPP27 at $c = 4.3$ g/L using an optical microscope with crossed polarizers.

Assuming the mesogens to be the cylindrical micelles of length $L = 500$ nm and diameter $d = 3.4$ nm, the critical concentration for a transition from the isotropic to the nematic phase can be estimated using Onsager theory[30] to be $\phi_{nemat} \approx 12$ g/L. Here, the density of the micelles has been set to $\rho = 1$ g/cm^3, which is justified according to $\rho = N_{rad} M_{dodecyl} [\pi R_{mic}^2 L_{mon}]^{-1} = 1.01$ g/cm^3, where $N_{rad} = 15$ is the radial aggregation number as determined from scattering,[7] $M_{dodecyl} = 169$ g/mol is the molar mass of each dodecyl group, $R_{mic} = 1.7$ nm is the radius of a micelle, and $L_{mon} = 1.2$ nm is the contour length of a monomer unit. Taking into account repulsive interactions between the negatively charged micelles, the nematic phase transition should be shifted to higher concentrations, since repulsive interactions are expected to renormalize the effective diameter with $d_{eff} > d$ and, according to Khokhlov,[31] to cause a twisting effect.

The experimentally determined isotropic → nematic transition point ($c \approx 1.1$ g/L) is significantly below the theoretically predicted one, which is hard to rationalize with the assumption of repulsive interactions. Instead, we have to assume attractive interactions between the negatively charged micelles, which confirms the results from static light scattering and viscometry, where a negative A_2 and a continuous increase of η_{red} with increasing c had been found.

SAXS. The assumption of cylindrical micelles is further confirmed by X-ray scattering of aqueous solutions of PPP27 as shown in Figure 9. All three scattering curves exhibit a maximum of $I(q)$ at $q_{max} \approx 2.9$ nm^{-1}, which has been shown to originate from reflections at the outer cylinder boundary and from which a diameter $d = 2\pi/q_{max} = 3.4$ nm of the cylindrical micelles can be obtained.[7] Above $c = 8$ g/L, there appears a second peak which becomes more pronounced with increasing concentration and which conforms to $q_{max} \propto c^{1/2}$.

The appearance of a structure forming process at higher concentrations of PPP27 in aqueous solution has

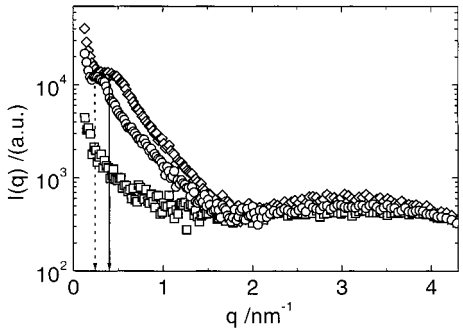

Figure 9. X-ray scattering patterns of aqueous solutions of PPP27 at $c = 5.47$ (□), 8.7 (○), and 15.7 g/L(◇). The structure peak at $c \geq 8.7$ g/L marks the appearance of a columnar phase of the cylindrical micelles (regime D).

already been reported by Rulkens et al., who studied the structure formation of PPPs in aqueous solution for $c > 10$ g/L.[32] They concluded that at these high concentrations PPPs form a columnar phase of cylindrical micelles which were assumed to have infinite length. This is schematically depicted in Figure 1, regime D. Hence, the structure peak is interpreted as a Bragg reflection. Assuming the distance between the lattice planes to be $d_{\mathrm{Bragg}} = 2\pi/q_{\mathrm{max}}$, the radial aggregation number

$$N_{\mathrm{rad}} = \frac{2}{\sqrt{3}} \frac{N_{\mathrm{A}} {d_{\mathrm{Bragg}}}^2 L_{\mathrm{mon}} c}{M_{\mathrm{mon}}} \qquad (10)$$

can be calculated to $N_{\mathrm{rad}} = 14$. This value is close to the result obtained from light scattering ($N_{\mathrm{rad}} = 15$) at very low concentrations.[7] Summarizing our results for PPP27 covering the concentration range $0.001 \leq c \leq 30$ g/L and those of Rulkens et al. covering $10 \leq c \leq 270$ g/L, we find that the cylindrical micelles which are formed by PPP27 in aqueous solution are stable with respect to their radial aggregation number over a concentration range of almost 6 decades.

PPP12. So far, we have mainly been concerned with the high molar mass sample PPP27. Now, the different patterns of structure formation of the low molar mass sample PPP12 shall briefly be discussed.

In the preceding paper,[7] we presented a study of the association pattern of two samples of PPP differing in molecular weight. The lower molar mass homologue polymer PPP12 exhibits the same chemical structure as PPP27 but with $M_{\mathrm{W}} \approx 12$ kg/mol. It has been shown that PPP12 in aqueous solution also forms cylindrical micelles of diameter $d = 3.4$ nm and length $L_{\mathrm{N}} = 104$ nm, which is about one-third of the length of the micelles formed by the polymer PPP27.[7] Since the cylindrical micelles from both PPPs have the same radial aggregation number, they both possess equal line charge density. Surprisingly, the aqueous solutions of PPP12 exhibit completely different characteristics and reflect much more typical polyelectrolyte behavior as is known from literature.[20,33,34] As shown in Figure 10, the reduced viscosity of aqueous solutions of PPP12 obeys a Fuoss−Strauss law (eq 2), as expected for polyelectrolytes where long-range Coulomb interactions increase with decreasing ionic strength.[17]

The differences between the two PPPs found in viscometry are confirmed by light scattering, where a positive second viral coefficient ($A_2 = 7.7 \times 10^5$ L mol g^{-2}) is found for dilute aqueous solutions of PPP12, whereas $A_2 = -1.84 \times 10^5$ L mol g^{-2} is negative for

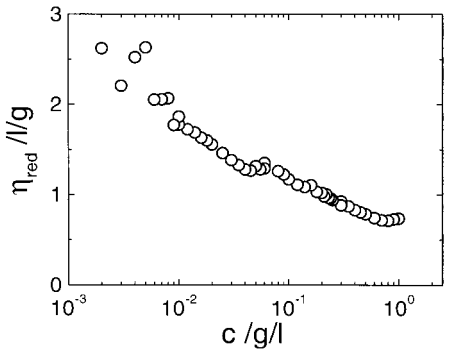

Figure 10. Reduced viscosity of a salt-free aqueous solution of PPP12.

PPP27.[7] Note that positive A_2 have also been found in methanol,[18] which displays a Fuoss−Strauss like reduced viscosity (Figure 2); this is expected for repulsive electrostatic interactions.[19] Since PPP12 forms cylindrical micelles with the same radial aggregation number as PPP27 but with length $L_{\mathrm{PPP12}} = 104$ nm, as compared to $L_{\mathrm{PPP27}} = 280$ nm, these results indicate that the overall interaction seems to be sensitive to the contour length of the polyion. The reason is not yet clear, but it might be argued that, since attractive interactions are presumably short range and hence require contact between the cylindrical macroions, the overall interaction will depend on the relation between rotational volume and electrostatic excluded volume of the rodlike polyions. Since the first scales as $V_{\mathrm{r}} \propto L^3$ and the second scales as $V_{\mathrm{e}} \propto L^{\alpha}$ with $\alpha < 3$,[20,35] attraction might be favored with increasing length. In a forthcoming publication we will present a detailed comparison between the structure formation properties of PPP12 and PPP27 and suggest a model that accounts for the influence of the contour length of a polyion on the overall interactions.

Summary and Conclusion

In this contribution we presented a detailed analysis of the structure formation properties of dodecyl-substituted poly(*p*-phenylene)sulfonates in salt-free aqueous solution. The polymers of the same structure form cylindrical micelles in aqueous solution which act as basic building blocks for higher ordered supramolecular structures. The results obtained from viscometry, light scattering, polarization microscopy, and X-ray scattering indicate a hierarchical structure formation for PPP27 that starts out from freely diffusing micelles at very dilute solutions, which further form ellipsoidal clusters with internal lyotropic ordering, a nematic phase, and finally a columnar phase of cylindrical micelles. The angular dependence of the scattering intensity in regime B (Figure 1) does not obey an Ornstein−Zernike law as predicted for fluctuating ordering states between the isotropic → nematic regime[27] but can be described by scattering functions which assume the existence of solid particles with a sharp boundary.

The formation and structure of the nematic clusters bears similarity to the predictions of a recent counterion condensation theory[2] for univalent counterions and the results of fluctuation theory[1] and MD simulations[3,4] in the presence of divalent counterions.

The negative A_2 as well as the isotropic → nematic phase transition at a concentration below the theoretically predicted one can be rationalized by assuming attractive interactions between the cylindrical micelles

of PPP27. This may be understood for rodlike polyions with line charge density above the Manning condensation threshold $\xi = l_B/b > 1$, where b is the closest distance between charges along the rod. Here, if two chains come sufficiently close, thermal fluctuations of the condensed counterions become coupled, resulting in van der Waals like attraction.[15] Oosawa suggested that the total force per unit length $f(R)$ between two parallel rods should be given to lowest order by

$$f(R) = k_B T\left(\frac{1}{Z^2 l_B R} - \frac{(Z\xi)^2}{1+(Z\xi)^2}\frac{1}{R^2}\right) \qquad (11)$$

where Z is the valency of counterions, ξ the charge parameter, and R the distance between the polyions.[36] In eq 11 the effect of correlated charge-density fluctuations is described by the second term, suggesting that dominating attractive interactions can also result in the case of monovalent counterions if ξ is sufficiently high. Assuming a radial aggregation number $N_{rad} = 15$, the line charge density of a cylindrical micelle is calculated to be $\xi = 18$, which is about 4 times that of DNA. From eq 11 it can be concluded that an increase in valency of counterions by a factor of x will have a similar effect on $f(R)$ as increasing ξ by a factor of x^2. Hence, we can rationalize fluctuation-induced attractive interactions between the micelles of PPPs also in the case of monovalent counterions. These attractive interactions are relevant for structure formation only in the case of cylindrical micelles, since in methanol, where no cylindrical micelles are found,[18] PPP27 exhibits polyelectrolyte behavior.

Acknowledgment. The authors thank I. Sprenger and R. Merkel from the Department of Physics at TU Munich for their help with electron microscopy. This work was supported by the Deutsche Forschungsgemeinschaft, Grants Ko1541 and Schu1047, and the Max-Planck Society.

References and Notes

(1) Ha, B. Y.; Liu, A. J. *Phys. Rev. Lett.* **1997**, *79*, 1289.
(2) Ray, J.; Manning, G. S. *Macromolecules* **2000**, *33*, 2901.
(3) Jensen, N. G.; Malsh, R. J.; Bruinsma, R. F.; Gelbart, W. M. *Phys. Rev. Lett.* **1997**, *78*, 2477.
(4) Stevens, M. J. *Phys. Rev. Lett.* **1999**, *82*, 101.
(5) Sogami, I.; Ise, N. *J. Chem. Phys.* **1984**, *81*, 6320.
(6) Ito, K.; Yoshida, H.; Ise, N. *Science* **1994**, *263*, 66.
(7) Bockstaller, M.; Köhler, W.; Wegner, G.; Fytas, G. *Macromolecules* **2000**, *34*, 6353.
(8) Rulkens, R.; Wegner, G.; Thurn-Albrecht, T. *Langmuir* **1999**, *15*, 4022.
(9) Rulkens, R.; Wegner, G.; Enkelmann, V.; Schulze, M. *Ber. Bunsen-Ges. Phys. Chem.* **1996**, *100*, 707.
(10) Bockstaller, M.; Köhler, W.; Wegner, G.; Vlassopoulos, D.; Fytas, G. *Macromolecules* **2000**, *33*, 3951.
(11) Strobl, G. *The Physics of Polymers;* Springer-Verlag: Berlin, 1997.
(12) Provencher, S. W. *Computer Phys. Commun.* **1982**, *27*, 229.
(13) Yamakawa, H. *Modern Theory of Polymer Solutions;* Harper and Row: New York, 1974.
(14) Cohen, J.; Priel, Z.; Rabin, Y. *J. Chem. Phys.* **1988**, *88*, 7111.
(15) Barrat, J. L.; Joanny, J. F. Theory of Polyelectrolyte Solutions. In *Polymeric Systems*; Prigogine, I., Rice, S. A., Eds.; John Wiley & Sons: New York, 1997.
(16) Cohen, J.; Priel, Z.; Rabin, Y. *J. Polym. Sci., Part C* **1988**, *13*, 85.
(17) Fuoss, R. M.; Strauss, U. P. *J. Polym. Sci.* **1948**, *3*, 176.
(18) Liu, T.; Rulkens, R.; Wegner, G.; Chu, B. *Macromolecules* **1998**, *31*, 6119.
(19) Odijk, T. The Theory of Light Scattering of Rod-Like Polyelectrolytes. In *Light Scattering*; Brown, W., Ed.; Clarendon Press: Oxford, 1996.
(20) Schmitz, K. S. *Macroions in Solution;* VCH Publishers: New York, 1993.
(21) Hunter, R. J. *Foundations of Colloid Science;* Oxford University Press: Oxford, 1995; Vol. 1.
(22) Pecora, R.; Berne, B. *Dynamic Light Scattering;* Wiley Interscience Publ.: New York, 1976.
(23) Higgins, J.; Benoit, H. *Polymers and Neutron Scattering;* Oxford University Press: Oxford, 1996.
(24) Schmitz, K. *An Introduction to Dynamic Light Scattering by Macromolecules*; Academic Press: New York, 1990.
(25) Einstein, A. *Ann. Phys.* **1910**, *33*, 1275.
(26) Perrin, F. *J. Chem. Phys.* **1942**, *10*, 415.
(27) de Gennes, P. G.; Prost, J. *The Physics of Liquid Crystals*, 2nd ed.; Clarendon Press: Oxford, 1990.
(28) Petekidis, G.; Vlassopoulos, D.; Fytas, G.; Fleischer, G. *Macromolecules* **1998**, *31*, 1406.
(29) Prost, J.; Williams, C. E. Liquid Crystals: Between Order and Disorder. In *Soft Matter Physics*; Daoud, M., Williams, C. E., Eds.; Springer-Verlag: Berlin, 1999.
(30) Onsager, L. *Ann. N.Y. Acad. Sci.* **1949**, *51*, 627.
(31) Khokhlov, A. R. *Liquid Crystallinity in Polymers;* VCH Publishers: New York, 1991.
(32) Rulkens, R.; Wegner, G.; Thurn-Albrecht, T. *Langmuir* **1999**, *15*, 4022.
(33) Sedlak, M.; Amis, E. J. *J. Chem. Phys.* **1992**, *96*, 817.
(34) Förster, S.; Schmidt, M. *Adv. Polym. Sci.* **1991**, *120*, 53.
(35) Gosh, S.; Li, X.; Reed, C. E.; Reed, W. F. *Biopolymers* **1991**, *30*, 1101.
(36) Oosawa, F. *Polyelectrolytes;* Marcel Decker: New York, 1971.

MA010027I